A Cable-Driven Switching-Legged Inchworm Soft Robot: Design and Testing

Xiaotian Chen, Paolo Stegagno, Chengzhi Yuan

***Abstract*— Inspired from biological systems, researchers are designing soft robots to replace conventional rigid body robots in many applications, including human-machine interaction, manipulation, medical instrumentation and wearable devices. In this paper, a cable-driven switching-legged inchworm-inspired soft robot is presented, in which motion is obtained by deforming the elastic body with actuated cables. The robot features low cost and fast manufacturing, as most of its components and molds for the soft body are 3D-printed, while electrical components are widely accessible on the market. Inspired by inchworm locomotion, we have developed a leg switching approach to control and exploit the difference of friction between the front and back of the robot to achieve basic motion capabilities. An extensive experimental campaign shows that the robot can perform basic movements (linear and angular motions) in multiple conditions as different surface frictions and slopes as well as following generic trajectories.**

I. INTRODUCTION

In recent years, soft robotics have attracted the interest of a growing number of researchers. Soft robots, due to their flexible bodies capable of achieving complex movements, are regarded as a possible alternative to traditional rigid body robots for motion in unstructured complex environments. Moreover soft robots can provide a more pleasant interaction experience to humans, or grip and manipulate fragile objects. In the development of a soft robot, the first challenge is to design an actuation mechanism [1], [2]. Most soft robots are actuated in one of three ways: fluidic actuation, variable length tendon, and electro-active polymer.

Fluidic actuation [3] is achieved by changing the fluid pressure (mostly air) inside the channels designed in the soft body of the robot (e.g., Pneu-Nets [4]) and motion is achieved by alternately inflating channels. This type of soft robot does not require any wire or electronic component mounted on the robot body, entirely soft. Variable length tendon and electro-active polymer are two types of materials which would deform under certain conditions. An example of variable length tendon actuator is shape-memory alloy (SMA). SMA materials deform due to a temperature-induced phase change [5], [6]. Electro-active polymers are materials that can be deformed by transduction mechanisms such as electro-static Maxwell pressure, ion migration induced swelling or other electrically stimulated transduction [7], [8]. These types of soft robots highly depend on the property of the tendons they employ. There are other ideas for actuation of soft robots, as vibration [9], chemical [10], light [11]. Another type of actuation is motor-controlled cable-driven systems which have been widely studied in manipulation [12], [13], [14], but limited in locomotion of soft robots. As mentioned in [15], motor-cable types of robots in general can reach higher velocity. [16] describes a high speed motor-cable robot, however, the motion of the robot is unstable particularly on the rotation, which may further affects accurate control. After deciding the actuation approach, soft robots need some strategies to control the motion. In their robot designs, many researchers have taken inspirations from biological systems as starfish [17], [18], snakes [19], worms [20], [21], and caterpillars [5], [22], [23]. More details on soft robot locomotion have been nicely summarized in [24].

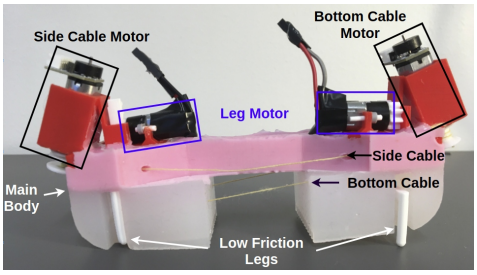

Fig. 1: Inchworm-like soft robot

In this paper, we present a new simple yet effective actuation idea: DC motors connected with cables to deform an elastic robot body, combined with a switching legged mechanism to enable locomotion of the soft robot. More specific, we present an inchworm-inspired robot based on this actuation idea (see Figure 1). We will show that the advantages of using motors with cables are i) the pulling length of the cable can be accurately controlled by the motor; ii) the pulling length is directly related to the robot travel distance. The robot design includes a deformable silicone rubber body (the pink portion as shown in Figure 1) which can be bent by changing the length of the side and bottom cable. When the cables are released, the main body will recover the initial shape thanks to its elasticity and stiffness. We employ a two-anchor crawling approach to achieve robot locomotion. By adding low friction legs to the high friction rubber body, we can create a friction difference between the two sides of the body that allows accurate control of the motion direction. This is achieved by switching the legs between hidden and extended positions with the leg motors.

This work was supported in part by the National Science Foundation under Grant CMMI-1929729.

X. Chen and C. Yuan are with the Department of Mechanical, Industrial and Systems Engineering, University of Rhode Island, Kingston, RI 02881, USA, e-mail: xiaotian_chen@my.uri.edu; cyuan@uri.edu

P. Stegagno is with the Department of Electrical, Computer and Biomedical Engineering, University of Rhode Island, Kingston, RI 02881, USA, e-mail: pstegagno@uri.edu

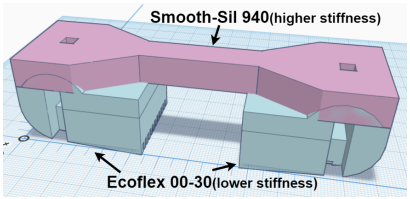

Fig. 2: 3D model of the main soft body. The blue part represents the first layer made with low stiffness silicone rubber (Ecoflex 00-30) The pink part represent the second layer which is made with higher stiffness silicone rubber (Smooth-sil 940).

The remainder of the paper is organized as follows. Section II describes the robot design and fabrication procedures. Section III presents experiments to verify the robot's performance. Section IV concludes the paper.

II. SOFT ROBOT DESIGN AND FABRICATION

The soft inchworm robot presented in Figure 1 consists of a two-layer silicone body, plastic legs, and motor-driven cables. We will specifically illustrate each part.

A. Robot design

The CAD design of the main body of the robot is shown in Figure 2. The bottom layer (blue) is made by a commonly used silicone rubber material (Ecoflex^{TM} 00-30). This material was selected to offer high friction with the ground, as the bottom layer serves as the feet of the inchworm. The top layer (pink) is made of another type of silicone rubber (Smooth-Sil^{TM} 940) which is stiffer than the first layer. This second layer is the main deformable component of the robot. When a force is applied at the two ends of the body, the middle bridge will hunch-up acting like the inchworm's undulating wave motion.

To achieve the bending force, we connect the two ends of the body with three cables. One long cable ("Bottom Cable" in Figure 1) starts at the Bottom Cable Motor, crosses through the whole bottom layer of the body, and comes back to the same motor. When the motor spins in one direction, the cable will roll up onto the motor's shaft reducing its length and the distance between two ends of the body. The body will, therefore, form an arch shape as shown in Figure 3(b). Two shorter cables ("Side Cable" in Figure 1) are placed on the left and right sides of the top silicone layer. These two are driven by the Side Cable Motor. When the side cable motor spins in one direction, one of the side cables will roll up onto the motor shaft, reducing its length. The other cable will unwind, becoming longer. This will cause the robot to bend on the left or right depending on the rotation direction.

Two white legs ("Low Friction Legs" in Figure 1), made with 3D printed PLA material, are controlled by two smaller DC motors ("Leg motor", one on each end of the body). The purpose of these legs is to modify the friction between the body and the ground. In fact, the Leg Motors are able to bring the legs into two positions: hidden position and extended position. When the legs are in hidden position, the rubber feet will be in contact with the ground, therefore there will

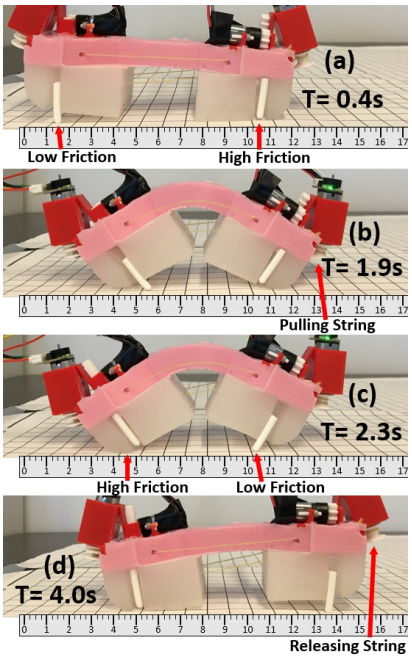

Fig. 3: The four steps for the forward motion of the soft robot (right side is the front part of the robot): (a) switch friction (front part has higher friction); (b) pull the bottom cable; (c) switch friction (back part has higher friction); (d) release the bottom cable.

be high contact friction between the rubber body and the ground. Conversely, when the legs are in extended position, they will touch the ground reducing the friction with the ground. Examples of legs in extended and hidden positions are provided in Figure 3(a), respectively the back (left) and front (right) legs.

B. Locomotion generation

In order to achieve the motion of the robot, legs and cables need to be actuated in a coordinated manner. To obtain forward motion (considering the front of the robot as the side with the bottom cable motor), the following steps must be performed (see Figure 3):

1) Set the front legs to hidden position and the back legs to extended position.
2) Pull the bottom cable to shrink the body until the vertical bending angle reaches a value θ.
3) Set the back legs to hidden position and the front legs to extended position.
4) Release the bottom cable to return the body to straight.

The angle θ (shown in Figure 4) is a parameter depending on the robot and cable length, and is linked to the length of a step of motion. In Section III, we will show more in detail this relationship.

Step 1 is designed to achieve a configuration in which the friction of the front of the body is higher than the friction of the back of the body. In step 2, due to the friction values selected with the leg configuration, the front of the body will

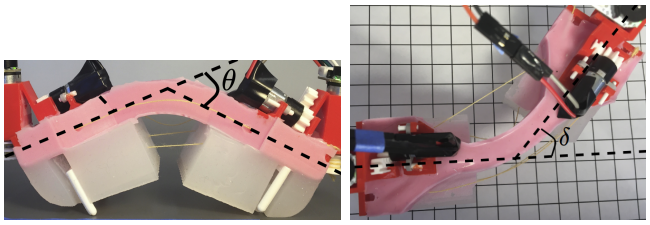

Fig. 4: Vertical bending angle θ (left), and horizontal bending angle δ (right)

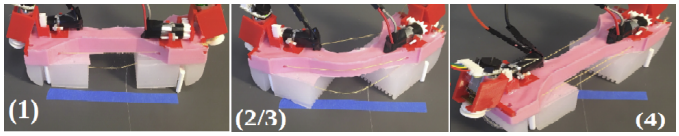

Fig. 5: The steps for the left turning motion of the soft robot (right side is the front part of the robot).

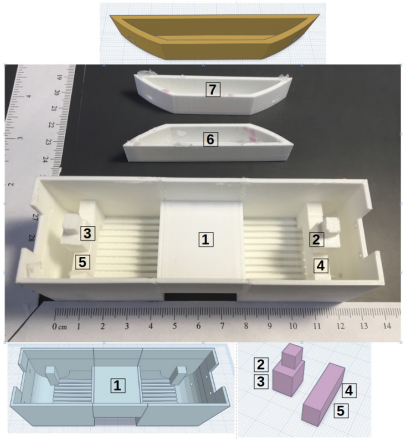

Fig. 6: 3D printed mold pieces. 1: Base of the mold. 2-5: Forming the hole of legs. 6-7: Shaping the central bridge of the body

stay still while the back will move forward. In step 3 the configuration of the legs is switched to obtain high friction in the back and low friction in the front. Therefore, in step 4 the front will move forward while the back will stay still. In order to achieve backward motion, we can follow the same procedure switching step 1 and 3.

A similar idea applies to left and right turn motion (see Figure. 5). One left(right) turn motion cycle is:

1) Set the back legs to hidden position and the front legs to extended position.
2) Pull the left(right) side cable to bend the body to the left(right) until the horizontal bending angle reaches a value δ.
3) Set the front legs to hidden position and the back legs to extended position.
4) Pull the right(left) side cable until the body is back to straight.

The angle δ (shown in Figure 4) is another parameter depending on the physical dimensions of the robot. During step 2 of the left(right) turn cycle, the front of the robot will move to the left(right) while the back, due to the higher friction, will act as an anchor. Similarly, during step 4, the back of the body will move to the right(left) while the front will stay still.

Linear and angular motions can be achieved simultaneously by combining the forward and turning motion. In this case, the robot is first preset to a specified horizontal bending angle δ by pulling the left(right) side cable, and then it will repeatedly perform the forward motion cycle.

C. Robot fabrication

As mentioned above the main body is made of two different types of silicone rubber. The desired shape is obtained by pouring the silicone rubber into a 3D-printed mold composed of 7 pieces (Figure 6). The first piece is the base of the mold. Pieces 2 to 5 are designed and mounted into piece 1 to create gaps to accommodate the legs. Finally, pieces 6 and 7 are designed to shape the central bridge of the body. The height and width of this bridge are two important design parameters as they affect the amount of force needed to deform the robot. On the base of piece 1, we have designed some straight grooves. These will create a special texture on the bottom surface of the body, which will increase the friction between the rubber and the ground. To obtain the channels for the cables across the body, we cut 8 pieces of plastic tubes (Tygon Tubing, 1/8in Outer Diameter), and place them in the mold. Four pieces of tube are placed near the bottom of the mold, two on each side. The rest of the tubes are placed at the same level as the mold piece 6 and 7, to form the channels for the side cables.

The motors are attached to the robot body through the use of 3D-printed motor holders (Figure 7, top right). These holders are embedded into the second layer of the body before the silicone rubber gets cured. In this way, the motor holders stay attached to the main body while the motors can be easily replaced. Other 3D printed parts required for this robot are the legs and gears (Figure 7, bottom right). The tooth shape on top of the legs and gears is designed to convert the motor's rotation into linear motion of the legs.

With all the mold pieces, tubes, and motor holders in their desired positions, the silicone rubber for the bottom layer is poured into the mold until it reaches the same height with the middle bridge of piece 1. After four hours of curing time, the top layer silicone rubber can be poured until it contacts the motor holders. It takes about 24 hours for the second layer to get completely cured. Finally, we carefully demold the body, replace the tubes with cables, and mount the legs, gears, and motors.

For the electronic part, the robot is controlled with a Romeo V2, an Arduino board with embedded motor drivers. All motors are Micro DC Gear Motors which can provide approximate 1 Nm torque. The cable motors are mounted with encoders while leg motors are not. All four motors are powered through constant 9V power.

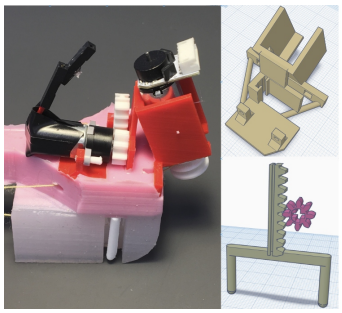

Fig. 7: The 3D printed legs, motor holder, and gears

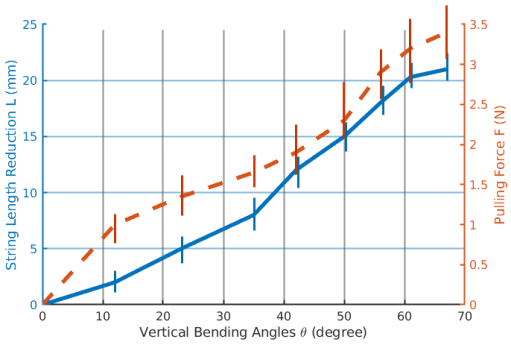

Fig. 8: x-axis is the vertical bending angle. Left y-axis (blue continuous line) is the cable pulling length (unit in mm). Right y-axis (red dotted line) is the measured pulling force (unit in N)

III. EXPERIMENTS

A. Preliminary experiment

Before motion experiments, we have experimentally investigated the relationship between the cable length, the bending angle, and the bending force. The bending force was measured by connecting the front end of the bottom cable to a Digital Force Meter and set the front leg at the hidden position while the back leg is at extended position. Then we fixed the front leg and pull the meter until the body reached the desired bending angles. With the motor encoders, we also measured the reduction of the cable length. With this setup, we measured the pulling force F and the cable length reduction L needed to achieve a bending angle θ of $12°$, $23°$, $35°$, $42°$, $50°$, $56°$, $61°$, and $67°$. The results plotted in Figure 8 suggest that F and L have a linear relationship with θ.

B. Experimental Setup

In order to evaluate the motion capabilities of the soft inchworm robot, we designed and conducted four experiments:

1) Evaluation of the forward motion by comparing the velocity on different surfaces and slopes.
2) Evaluation of the turning motion by comparing the rotation angle on different surfaces and slopes.
3) Combined linear and turning motion with different horizontal bending angles δ.
4) Motion along a predetermined trajectory.

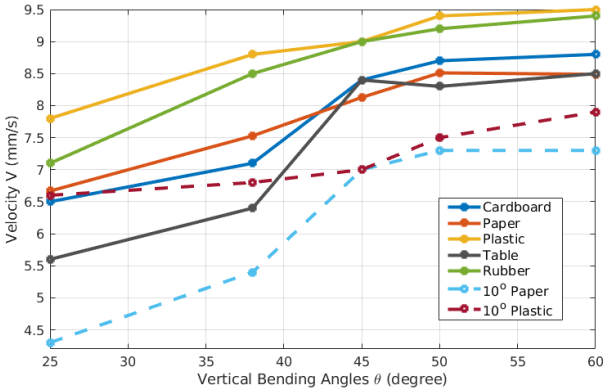

Fig. 9: Comparison of the linear velocity V in 7 different environmental conditions.

In the first experiment, the forward motion of the robot was tested under 7 environmental conditions: 0 degree slope on five surfaces (cardboard, paper, smooth plastic, painted table, and smooth rubber), 10 degree slopes on paper and smooth plastic. Each experiment was repeated for five different bending angles $\theta = 25°, 38°, 45°, 50°, 60°$ to evaluate the effect of this parameter on the velocity of the robot. In each trial, the robot would perform six cycles of forward motion. Through measurements of total traveling distance and time, we would then compute the velocity.

In the second experiment, we tested the left turning motion under four different environmental conditions: 0 and 10 degree slopes on paper and plastic surface. Each test was repeated for five horizontal bending angles δ. In each trial, the robot would perform three cycles of turning motion. At the end, we measured the total rotation angle of the robot.

In the third experiment, the robot performed the combined forward and turning motion with four different horizontal bending angles $\delta = 25°, 35°, 45°, 55°$. Each test was repeated five times with six cycles of motion.

In the fourth experiment, the robot was driven on surface of the table to follow a Z-shape trajectory.

C. Experimental Result

Figure 9 shows the result of experiment 1. The x-axis is the robot vertical bending angles θ and the y-axis is the linear velocity V (mm/s). Each line in the plot represents one of the environmental conditions. The plot shows that in general higher bending angles θ allow the robot to move faster. However, when θ becomes greater than $50°$, the velocity stops to increase.

The comparison among the seven different conditions shows that different surface materials and slopes will influence the friction between the legs and surface, and further, will affect the locomotion of the robot. According to Figure 9, the velocities on the smooth plastic surface are the highest which is due to its lowest friction among other materials. As expected, the velocity decreases when the slope of the surface increases because the elastic force of the robot's body is not strong enough to bring it back to straight completely. In fact, during step 4 of the forward motion, when the cable is

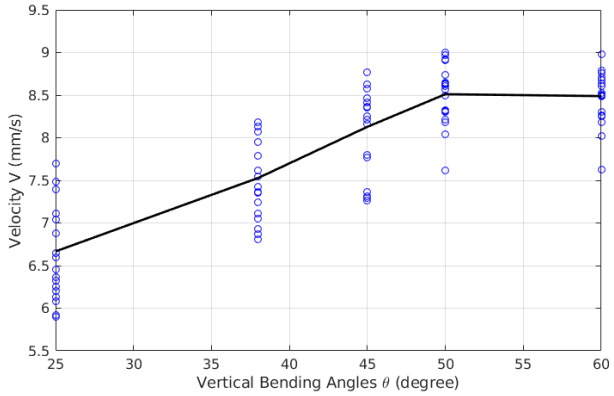

Fig. 10: The Linear velocity V with respect to the bending angle θ on 100 trials. Each blue circle represents one trail and the black line is the mean value.

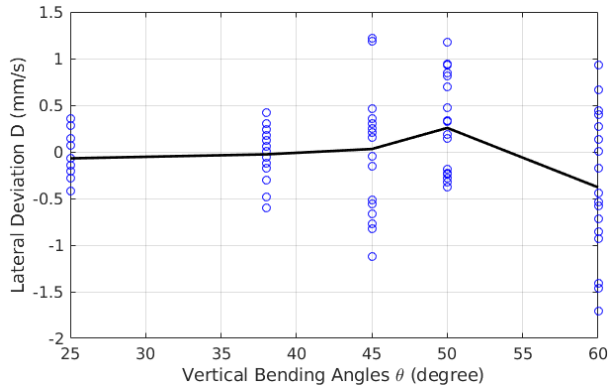

Fig. 11: The lateral deviation D from a straight line with respect to the bending angles θ on 100 trials. Each blue circle represent one trial and the black line is the mean value.

released the elastic force of the deformed body is supposed to push the front part of the body forward. In the meantime, when on the slope there will be friction with partial gravity against this elastic force. As the bending angle decreases to the point where the elastic force balanced with the friction, the front part of the body will stop moving, even though the robot body will still have some small bending angle.

To further characterize the motion properties of the inch-worm robot, we have performed 100 trials on the flat paper surface, 20 for each value of θ. In these trials we have also measured the lateral deviation of the robot from straight line motion. The velocities V and lateral deviations D for all trials are reported in Figure 10 and 11 respectively. The values of mean and variance of V and D are reported in Table I. The variance of the robot velocity decreases slightly with θ, while the variance of the lateral deviation D increases. As shown in Figure 10, the velocity unusually decreases at the highest bending angle (i.e., 60°). This may be caused by the fact that high degree of bending angle takes more time to reach but the forward distance does not get equivalent increases. Based on these results, we choose to set $\theta = 50°$ in the third and fourth experiments.

The results of experiment 2 are shown in Figure 12. The

TABLE I: Forward motion evaluation on the paper surface. The average of the results of 20 trails on each bending angle.

Vertical Bending Angle (degree)	25	38	45	50	60
Pulling Force (N)	1.4	1.8	2	2.3	3.2
Distance (mm)	95.3	125	159	181	191
Time (s)	14.3	16.7	19.6	21.2	22.5
Velocity V (mm/s)	6.7	7.5	8.1	8.5	8.4
Standard Deviation of the Velocity	0.57	0.43	0.48	0.34	0.31
Lateral Deviation D	-0.07	-0.037	0.03	0.026	-0.38
variance of the Lateral Deviation	0.204	0.281	0.622	0.505	0.717

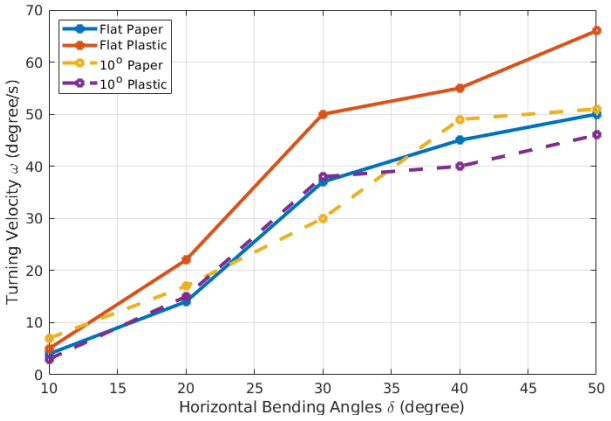

Fig. 12: Turning speed analysis comparing between 4 different surfaces and slopes

turning velocity increases substantially when the horizontal turning angle δ is increased from 20° to 30°. When releasing the cable, because of the friction, the body of the robot would not recover back to perfectly straight. So low horizontal bending angles proved to be less effective for the turning motion. In experiment 4, the horizontal bending angle is therefore set to 30°.

The cross-comparison among different surfaces and slops provides similar results as the forward motion case. Flat and low friction surfaces give the highest moving velocity.

Figure 13 shows the results of experiment 3. The plots represent the average trajectories and final poses of the five tries for each of the tested horizontal bending angles δ. The robot starts in $(0, 0)$ with the front direction pointing to the right. The dashed line represent the trajectories while the arrows represent the robot final orientation. From this Figure, we can conclude that higher horizontal bending angles give smaller turning radii. However, the total traveled distance and rotation with $\delta = 45°, 55°$ are all less than the results with $\delta = 35°$. This happens because when the soft body is already horizontally bent, vertical bending becomes harder and unstable.

For experiment 4, the robot was driven to follow a Z-shaped trajectory. The robot is manually controlled with four direction commands (forward, backward, left, right). The motion parameters were set to $\theta = 50°$ and $\delta = 30°$. The results are depicted in Figure 14. The red arrows represent

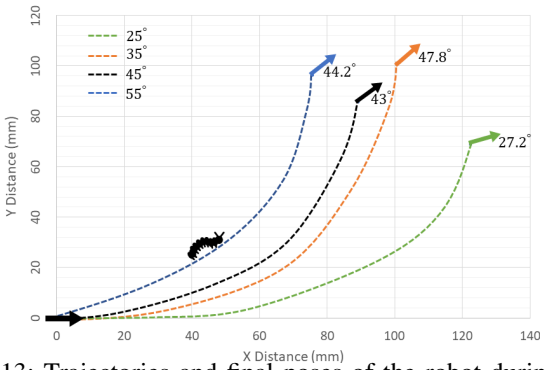

Fig. 13: Trajectories and final poses of the robot during the 6 cycles of forward motion. The robot is fixed to 4 different horizontal bending angles $\delta = 25°, 35°, 45°, 55°$.

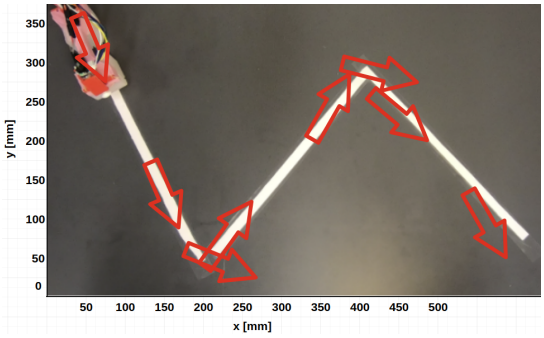

Fig. 14: Result of experiment 4: a Z-shape trajectory following. The red arrow represents the robot position and direction every 30 seconds. The white line is the desired trajectory.

the robot pose every 30 seconds. The white line is the desired trajectory. It takes 3 minutes and 35 seconds to finish this trajectory with 33 forward motion cycles, 7 turns left motion cycles, and 9 turn right motion cycles.

IV. CONCLUSIONS

In this work, we presented a novel actuation approach (cable-driven) for soft robot design, combined with a switching-legged two-anchor crawling mechanism to control soft robot locomotion. The cables are pulled by motors to deform the elastic robot body into desired shapes (vertical bending and horizontal bending). The two-anchor crawling is achieved by switching between two types of robot-to-ground contact surface (plastic and rubber). We tested the robot on multiple surfaces and slopes with promising results.

REFERENCES

[1] C. Lee, M. Kim, Y. J. Kim, N. Hong, S. Ryu, H. J. Kim, and S. Kim, "Soft robot review," *International Journal of Control, Automation and Systems*, vol. 15, no. 1, pp. 3–15, 2017.

[2] C. Laschi, B. Mazzolai, and M. Cianchetti, "Soft robotics: Technologies and systems pushing the boundaries of robot abilities," *Sci. Robot*, vol. 1, no. 1, p. eaah3690, 2016.

[3] D. Rus and M. T. Tolley, "Design, fabrication and control of soft robots," *Nature*, vol. 521, no. 7553, p. 467, 2015.

[4] K. M. de Payrebrune and O. M. O'Reilly, "On constitutive relations for a rod-based model of a pneu-net bending actuator," *Extreme Mechanics Letters*, vol. 8, pp. 38–46, 2016.

[5] T. Umedachi and B. A. Trimmer, "Design of a 3d-printed soft robot with posture and steering control," in *2014 IEEE International Conference on Robotics and Automation (ICRA)*. IEEE, 2014, pp. 2874–2879.

[6] T. Umedachi, V. Vikas, and B. A. Trimmer, "Highly deformable 3-d printed soft robot generating inching and crawling locomotions with variable friction legs," in *2013 IEEE/RSJ international conference on Intelligent Robots and Systems*. IEEE, 2013, pp. 4590–4595.

[7] K. Takagi, M. Yamamura, Z.-W. Luo, M. Onishi, S. Hirano, K. Asaka, and Y. Hayakawa, "Development of a rajiform swimming robot using ionic polymer artificial muscles," in *2006 IEEE/RSJ International Conference on Intelligent Robots and Systems*. IEEE, 2006, pp. 1861–1866.

[8] Y. Almubarak and Y. Tadesse, "Twisted and coiled polymer (tcp) muscles embedded in silicone elastomer for use in soft robot," *International Journal of Intelligent Robotics and Applications*, vol. 1, no. 3, pp. 352–368, 2017.

[9] B. Berger, A. Andino, A. Danise, and J. Rieffel, "Growing and evolving vibrationally actuated soft robots," in *Proceedings of the Companion Publication of the 2015 Annual Conference on Genetic and Evolutionary Computation*, 2015, pp. 1221–1224.

[10] R. F. Shepherd, A. A. Stokes, J. Freake, J. Barber, P. W. Snyder, A. D. Mazzeo, L. Cademartiri, S. A. Morin, and G. M. Whitesides, "Using explosions to power a soft robot," *Angewandte Chemie International Edition*, vol. 52, no. 10, pp. 2892–2896, 2013.

[11] M. Rogóż, H. Zeng, C. Xuan, D. S. Wiersma, and P. Wasylczyk, "Light-driven soft robot mimics caterpillar locomotion in natural scale," *Advanced Optical Materials*, vol. 4, no. 11, pp. 1689–1694, 2016.

[12] C. Li, X. Gu, and H. Ren, "A cable-driven flexible robotic grasper with lego-like modular and reconfigurable joints," *IEEE/ASME Transactions on Mechatronics*, vol. 22, no. 6, pp. 2757–2767, 2017.

[13] V. Slesarenko, S. Engelkemier, P. I. Galich, D. Vladimirsky, G. Klein, and S. Rudykh, "Strategies to control performance of 3d-printed, cable-driven soft polymer actuators: From simple architectures to gripper prototype," *Polymers*, vol. 10, no. 8, p. 846, 2018.

[14] F. Renda, M. Giorelli, M. Calisti, M. Cianchetti, and C. Laschi, "Dynamic model of a multibending soft robot arm driven by cables," *IEEE Transactions on Robotics*, vol. 30, no. 5, pp. 1109–1122, 2014.

[15] T. Umedachi, V. Vikas, and B. Trimmer, "Softworms: the design and control of non-pneumatic, 3d-printed, deformable robots," *Bioinspiration & biomimetics*, vol. 11, no. 2, p. 025001, 2016.

[16] V. Vikas, E. Cohen, R. Grassi, C. Sözer, and B. Trimmer, "Design and locomotion control of a soft robot using friction manipulation and motor–tendon actuation," *IEEE Transactions on Robotics*, vol. 32, no. 4, pp. 949–959, 2016.

[17] H. Jin, E. Dong, G. Alici, S. Mao, X. Min, C. Liu, K. Low, and J. Yang, "A starfish robot based on soft and smart modular structure (sms) actuated by sma wires," *Bioinspiration & biomimetics*, vol. 11, no. 5, p. 056012, 2016.

[18] S. Mao, E. Dong, H. Jin, M. Xu, S. Zhang, J. Yang, and K. H. Low, "Gait study and pattern generation of a starfish-like soft robot with flexible rays actuated by smas," *Journal of Bionic Engineering*, vol. 11, no. 3, pp. 400–411, 2014.

[19] C. D. Onal and D. Rus, "Autonomous undulatory serpentine locomotion utilizing body dynamics of a fluidic soft robot," *Bioinspiration & biomimetics*, vol. 8, no. 2, p. 026003, 2013.

[20] S. Seok, C. D. Onal, K.-J. Cho, R. J. Wood, D. Rus, and S. Kim, "Meshworm: a peristaltic soft robot with antagonistic nickel titanium coil actuators," *IEEE/ASME Transactions on mechatronics*, vol. 18, no. 5, pp. 1485–1497, 2012.

[21] Z. G. Joey, A. A. Calderón, and N. O. Pérez-Arancibia, "An earthworm-inspired soft crawling robot controlled by friction," in *2017 IEEE International Conference on Robotics and Biomimetics (ROBIO)*. IEEE, 2017, pp. 834–841.

[22] Z. Deng, M. Stommel, and W. Xu, "A novel soft machine table for manipulation of delicate objects inspired by caterpillar locomotion," *IEEE/ASME Transactions on Mechatronics*, vol. 21, no. 3, pp. 1702–1710, 2016.

[23] H.-T. Lin, G. G. Leisk, and B. Trimmer, "Goqbot: a caterpillar-inspired soft-bodied rolling robot," *Bioinspiration & biomimetics*, vol. 6, no. 2, p. 026007, 2011.

[24] M. Calisti, G. Picardi, and C. Laschi, "Fundamentals of soft robot locomotion," *Journal of The Royal Society Interface*, vol. 14, no. 130, p. 20170101, 2017.